

AL11100 989092

NBS
PUBLICATIONS

NBSIR 80-2023

Micromechanisms of Crack Growth in Ceramics and Glasses in Corrosive Environments

S. M. Wiederhorn, E. R. Fuller, Jr. and R. M. Thomson

Fracture and Deformation Division
Center for Materials Science
National Bureau of Standards
U.S. Department of Commerce
Washington, D.C. 20234

May 1980

Interim Report

Prepared for
Office of Naval Research
Department of the Navy
Hampton, VA

QC
100
.U56
No. 80-2023
1980
c.2

NBSIR 80-2023

NATIONAL BUREAU OF STANDARDS
LIBRARY

**MICROMECHANISMS OF CRACK
GROWTH IN CERAMICS AND
GLASSES IN CORROSIVE ENVIRONMENTS**

JUL 10 1980
not. acc. - CIRC.
QC
100
U56
No. 80-2023
1980
C.2

S. M. Wiederhorn, E. R. Fuller, Jr. and R. M. Thomson

Fracture and Deformation Division
Center for Materials Science
National Bureau of Standards
U.S. Department of Commerce
Washington, D.C. 20234

May 1980

Interim Report

Prepared for
Office of Naval Research
Department of the Navy
Arlington, VA



U.S. DEPARTMENT OF COMMERCE, Philip M. Klutznick, *Secretary*

Luther H. Hodges, Jr., *Deputy Secretary*

Jordan J. Baruch, *Assistant Secretary for Productivity, Technology, and Innovation*

NATIONAL BUREAU OF STANDARDS, Ernest Ambler, *Director*

Micromechanisms of Crack Growth in Ceramics and Glasses
in Corrosive Environments

S.M. Wiederhorn, E.R. Fuller, Jr., and R. Thomson
National Bureau of Standards
Washington, D.C. 20234

ABSTRACT

At normal temperatures and pressures, water is known to have a strong influence on the strength of ceramics and glasses. Behaving as a stress-corrosion agent, water causes these materials to fail prematurely as a consequence of subcritical crack growth. A basic premise of this paper is that stress-corrosion cracking of ceramics is a chemical process that involves a stress-enhanced chemical reaction between the water and the highly stressed ceramic near the crack tip. Plastic deformation is believed to play no role in this fracture process. After a brief survey of chemical reaction rate theory, the basic rate equation from this theory is modified to reflect physical and chemical processes that occur at crack tips. Modification of the rate equation is based on the assumption that the crack tip can be modelled as an elastic continuum, an assumption that is supported by a simple atomistic model of crack growth. When tested against experimental data collected on glass, the theory was found to be consistent with measurements of the crack-growth dependence on temperature, applied stress intensity factor, and concentration of reactive species in the environment.

1. Introduction

In the presence of corrosive environments, structural materials often experience delayed failure when subjected to mechanical loads. These environments react chemically or physically with the stressed material causing subcritical crack growth that results in structural failure when the crack has grown to a critical size. The time to failure is the total time required for the nucleation and growth of a crack to a critical size. Known as stress corrosion cracking, this process is superficially the same for ceramic, metallic, and polymeric materials, since all three kinds of material exhibit similar types of delayed failure curves. Failure occurs most rapidly at high loads. Below a critical value of the load known as the stress corrosion limit, failure does not occur regardless of the time that the load is supported.

Despite these similarities in fracture behavior, the mechanisms of fracture for the three types of materials differ greatly. Polymers and metals have plastic zones at their crack tips, so that stress corrosion cracking of these materials involve the generation, propagation, and fracture of plastic zones in these materials. By contrast brittle materials such as Al_2O_3 , SiC or Si do not have plastic zones at their crack tips, so that the fracture of these materials must be explained by mechanisms that preclude the occurrence of plastic deformation [1,2]. It is these types of materials that are discussed in this paper. Since these materials are treated as ideally brittle solids, a short description of recent experiments examining the crack-tip structure is presented to support this proposed model of fracture.

Evidence for the absence of a plastic zone at the tips of cracks in brittle, crystalline materials has been obtained by the use of transmission electron

microscopy [1,2]. Examination of thin foils of Al_2O_3 , SiC, Ge and Si that contain cracks has shown the crack tips to be devoid of mobile dislocations when the cracks are introduced into the foils at low temperatures.

Furthermore, removal of the driving force for fracture results in spontaneous crack healing of cracks in these materials, which suggests that in the absence of an opening mode force, the fracture surfaces can become reattached by strong molecular forces. At elevated temperatures, however, where plastic deformation is expected, mobile dislocations are observed at crack tips.

Although inorganic silicate glasses are an important class of brittle material, the technique of transmission electron microscopy cannot be applied because of the lack of long-range order in these materials. However, recent transmission electron microscopy studies on crystalline quartz, which has the same type of atoms and atomic bonding as glass, also indicate an absence of plastic deformation during fracture [3]. In addition, since crack healing has been observed in glass [4], and since the fracture toughness of glass [5] is similar to that of silicon [6] (which has the same hardness and exhibits no plastic deformation during fracture) it is probable that inorganic silicate glasses also fracture in a completely brittle manner.

The consequence of completely brittle behavior is the development high strains at crack tips prior to crack propagation. Bonds at the crack tip in a completely brittle solid are strained until they reach a state of instability at which point fracture occurs. The level of elastic strains that can be achieved in brittle materials can be estimated from strength measurements on silica glass fibers and rods [7,8]. Because test specimens of silica glass can be made by fusion

techniques, their surface are highly perfect, lacking the small flaws and cracks that act as stress concentrators in normal silica glass artifacts. Consequently, silica glass can be subjected to stresses as high as ~ 14 GPa (2×10^6 psi) in vacuum or in other inert environments. Based on a Young's modulus of 75 GPa, a stress of this magnitude corresponds to an elastic strain before fracture of approximately 20 percent. Because test specimens used in these measurements undoubtedly contain structural defects that are several times the size of the holes in the glass network structure, strains in the vicinity of fracture origins must be even greater than 20 percent.

Strained bonds at crack tips of brittle materials can break for two reasons: thermal fluctuations that are normally present in materials can cause individual bonds to stretch beyond their cohesive limit so that they rupture; or reactive environments can preferentially cleave highly strained bonds by chemical attack. Subcritical crack growth resulting from either process can be described in terms of reaction rate theory, and theoretical approaches of this type have been taken by a number of authors [9-18]. Bond rupture can also be rationalized in terms of chemical reactions, which for certain types of reactions have a great deal in common with fracture. Although the chemical approach to fracture is also based on reaction rate theory (so that the two are compatible), expressions for the rupture process can be related to the structure of brittle materials in a simple manner. The purpose of this paper is to treat the rupture process at crack tips as a chemical reaction and to show how parameters normally obtained from fracture mechanics experiments can be related to parameters that are normally used to describe chemical

reactions. In particular it will be shown that the slope of the stress corrosion curve can be related to the activation volume obtained from chemical kinetics studies. Since activation volumes are particularly amenable to structural interpretation, this relation permits crack growth data to be discussed directly in terms of the atomic structure of the crack tip. The chemical approach to fracture is consistent with the statistical mechanics models developed by other authors [16].

2. Chemical Reaction Rate Theory

A brief review of the chemical approach to reaction rate theory is presented for the reader who is unfamiliar with this subject. A complete description of reaction rate theory can be found in reference 19.

The thermodynamic formulation of reaction rate theory is based on the assumption that reactants are in a state of equilibrium with an activated complex that forms during the reaction. The activated complex then decomposes to form the reaction products. Based on this assumption it can be shown that the rate coefficient, k_r , for a single step reaction is given by [20]:

$$k_r = \left[\kappa \frac{kT}{h} \exp(-\Delta G^\ddagger/RT) \right] \left[\prod_i f_i / f^\ddagger \right], \quad (1)$$

where k is Boltzmann's constant, h is Planck's constant, R is the gas constant and f_i and f^\ddagger are the activity coefficients of the reactants and the activated complex, respectively. The parameter κ is the so-called transmission coefficient which accounts for the fact that for some reactions, not all activated complexes decompose into reaction products. For most reactions, κ is equal to unity.

The free energy of activation can be expressed in terms of chemical potentials for the reaction referred to their standard state:

$$\Delta G^\ddagger = \mu^\ddagger - \sum_i \mu_i \quad (2)$$

Hence, ΔG^\ddagger is the difference in partial molar free energy between the initial and activated state of reaction, all referred to their standard state. As such, ΔG^\ddagger can be expressed in terms of other partial molar quantities:

$$\Delta G^\ddagger = -T\Delta S^\ddagger + \Delta E^\ddagger + P\Delta V^\ddagger \quad (3)$$

where ΔS^\ddagger is the activation entropy, ΔE^\ddagger is the activation energy, and ΔV^\ddagger is the activation volume, each of these quantities being determined from the change in state from the initial to the activated state of reaction.

The temperature dependence of a chemical reaction is characterized by the enthalpy of reaction ($\Delta H^\ddagger = \Delta E^\ddagger + P\Delta V^\ddagger$):

$$\partial(\ln k_r)/\partial T = 1/T + \Delta H^\ddagger/RT^2, \quad (4)$$

provided the activity coefficients are independent of temperature. Usually, the temperature dependence of the rate constant is determined from a plot of $\ln k_r$ versus $1/RT$, and the slope of the line is reported as the experimental activation energy, E_{exp} :

$$E_{\text{exp}} = \Delta H^\ddagger + RT \quad (5)$$

Since activation energies for chemical reactions range from ~ 10 to ~ 100 kcal/mol [19], RT is usually small relative to ΔH^\ddagger and can be neglected.

The pressure dependence of chemical reactions is characterized by the activation volume, ΔV^\ddagger .

$$\partial(\ln k_r)/\partial P = \Delta V^\ddagger/RT \quad (6)$$

Since the activation volume is the difference in partial molar volume between the reactants and the activation complex, it can be modelled by changes in molecular dimensions as the reaction goes through the activated state.

Two important effects are usually considered in estimating the activation volume [21]. The first effect has to do with structural changes that occur during the reaction (i.e., whether bonds are being formed or broken) and with the number of molecules taking place in the reaction. In liquids, unimolecular bond rupture always leads to a positive activation volume, whereas bimolecular bond formation always leads to a negative activation volume [20,22,23]. The second effect has to do with the formation,

destruction or alteration of charge during chemical reactions. Charges alter the volume of the solvent through the process of electrostriction, and the change in volume of the solvent must be added to the change in volume of the reacting species as they become activated. Quantitative approximations developed to account for electrostriction indicate large negative volume changes ($-10 \text{ cm}^3/\text{mole}$) if charge formation occurs during the activation step. As a general rule, the portion of the activation volume due to electrostriction is larger than that due to structural changes when reactions take place in liquid solvents [22]:

For a wide variety of chemical reactions, activation volumes are found to range from $\sim -20 \text{ cm}^3/\text{mole}$ to $\sim 10 \text{ cm}^3/\text{mole}$ [20,22,23]. An interesting observation made by Laidler [19] is that the activation entropy, ΔS^\ddagger , appears to be related linearly to the activation volume, which can be used to obtain an estimate of the activation entropy. Activation volumes are also used to obtain information on the type of reaction occurring in a liquid system. As noted by Laidler [19], reactions can be classified into three types, "slow", "normal" and "fast", according to their volume of activation. Slow reactions often involve the formation of opposite charges, or the approach of like charges and have large negative volumes of activation. In normal reactions, electrostatic effects are unimportant, and volumes of activation are usually small and negative. Fast reactions often involve the approach of opposite charges or the spread of like charges and have positive volumes of activation. Since chemical bonds are stretched and broken during fracture, fast reactions with positive activation volumes are clearly most applicable for characterizing crack-growth rates.

3. Application of Chemical Theory to Fracture

The chemical reaction rate theory discussed in the previous section was developed for reactions occurring in a liquid environment. To apply these ideas to fracture, two modifications to the above equations are necessary. First, since reactions at a crack tip occur in the presence of high stress fields, stresses rather than pressures have to be incorporated into the external work term ($P\Delta V^\ddagger$ of eqn. 3). Second, since the crack tip can be modelled as a highly curved surface, effects of surface curvature on chemical potential must be considered.

The two modifications discussed in this section are developed in the same spirit as that used in the previous section. This development is supported, however, by a more rigorous statistical mechanics formalism for the advance of a crack by thermal fluctuations in a solid [16]. The activation energy barrier for the advancing crack involves the reaction of the chemically interacting species with the atoms of the solid whose bonds are about to break at the tip. The normal chemical reaction of the gas with the solid atoms at the crack tip will be drastically altered by the fact that the bonds at the crack tip are violently stretched. Therefore, the activation energy will depend upon the stress in a complex manner which can only be calculated in terms of specific interatomic forces and configurations. Nevertheless, in section 6 we show that an activation volume can be derived for the crack-tip bond rupture event in a discrete model of a solid, which supports the development in this section. Accordingly, here we follow the lead of Charles and Hillig [24] and write an expression for ΔG^\ddagger which is constructed from considerations based on continuum stress and liquid surface tension arguments, and from this expression derive an activation volume for crack growth. The expression thus derived will then be

compared to experiments. In section 6 the expression is shown to be equivalent to the discrete atomistic model analysis.

Accordingly, the crack tip is assumed to have an elliptical shape, with a curvature equal to ρ . The stress at this crack tip, σ , can be evaluated from the continuum elasticity solution of an elliptically shaped hole subjected to an applied stress normal to the crack plane. In fracture mechanics terms the crack-tip stress is related to the applied stress intensity factor, K_I , and the crack-tip radius, ρ , by the following equation [25]:

$$\sigma = 2K_I / (\pi\rho)^{1/2} \quad (7)$$

Since the crack-tip stress lies normal to the fracture plane, it also lies normal to the chemical bonds that are broken during crack propagation, and hence, can be considered as a negative pressure applied to the atoms in the vicinity of the crack tip. By substituting $-\sigma$ for P in eqn. 3, the reaction rate equation can be expressed in terms of the driving force for fracture, K_I . As will be shown below, the volume of activation can be determined from crack propagation curves obtained by fracture mechanics techniques. Activation volumes determined in this manner are equal to the partial molar volume difference between the activated complex and the stressed solid that is undergoing reaction. Because the corrosive environment is not subjected to stress, it does not contribute to the activation volume. This is a significant difference in behavior between chemical reactions in a pressurized fluid, and reactions at the surface of a stressed solid.

Surface curvature can also modify the rate of chemical reaction by modifying the chemical potential of reactants at the surface. The dependence of chemical potential on surface curvature is given by the following equation [26]:

$$\mu = \mu_0 + \gamma V/\rho \quad (8)$$

where μ is the chemical potential at a surface of curvature, ρ , and μ_0 is the chemical potential at a flat surface. The surface free energy of the solid is γ and the partial molar volume of the material undergoing reaction is V . For material undergoing reaction at a crack tip, the surface curvature is negative. Surface curvature is expected to modify the chemical potential of the activated complex (since it lies on the surface) and the chemical potential of the initial reactants that form part of the solid, but not the chemical potential of the corrosive species that are reacting with the solid because they are not part of the surface. The effect of curvature on the activation free energy is obtained by substituting eqn. 8 into eqn. 2:

$$\Delta G^\ddagger = \mu_0^\ddagger - \sum_i \mu_0^i - (\gamma^\ddagger V^\ddagger - \gamma V)/\rho \quad (9)$$

The fact that ρ is negative is taken into account in eqn. 9 by use of a minus sign in front of the term in parentheses.

By modifying eqn. 3 to account for crack-tip curvature and crack-tip stress, the following equation is obtained for the free energy of activation:

$$\Delta G^\ddagger = -T\Delta S^\ddagger + \Delta E^\ddagger - [2K_I/(\pi\sigma)]^{1/2} \Delta V^\ddagger - (\gamma^\ddagger V^\ddagger - \gamma V)/\rho. \quad (10)$$

From eqn. 10, we see that the application of a load to a solid containing a crack accelerates the reaction provided the activation volume for the reaction is positive. If the activation volume is negative, the reaction at the crack tip will be inhibited by the application of an applied load, and subcritical crack growth will probably not occur. The effect of curvature on the reaction will depend on the relative values of the surface free energies and of molar volumes in eqn. 10.

4. Experimental Data

A considerable body of experimental data has been collected to characterize subcritical crack growth in glasses and ceramics. By far, the largest amount of data has been collected on commercial glasses, for which the crack growth rate has been characterized as a function of applied stress intensity factor, temperature and environment. Data have also been obtained on single crystal aluminum oxide [27] and on alkaline earth fluorides [28], however these data are not as reliable, nor as extensive as those obtained on glass and will not be discussed in this paper. Data obtained on polycrystalline ceramic materials will also not be discussed because of complications introduced by the polycrystalline nature of these materials.

Crack velocity studies on soda-lime-silica glass in nitrogen gas containing water vapor indicate three regions of crack growth, Figure 1, that depend on stress intensity factor and on percent relative humidity of the environment [29]. In region I, the crack growth rate is proportional to the partial pressure of the water in the gas for a given stress intensity factor, and the slope of the curves is approximately equal to $0.1/RT$ in MKS units. In region II the crack growth rate is weakly dependent on the stress intensity factor, and is linearly proportional to the relative humidity of the water in the nitrogen gas. In region III the crack growth rate depends only on the applied stress intensity factor; the slope of the curve is approximately equal to $0.9/RT$. Within experimental error, data obtained on soda-lime-silica glass in vacuum at room temperature [30] are identical to the region III data shown in Figure 1, which suggests that region III crack growth represents a fracture process that is environment independent.

Studies conducted on a variety of commercial glasses in water indicate that the data obtained are similar to those obtained for region I crack propagation in nitrogen gas [24]. The position of the crack propagation curve is sensitive to temperature, crack propagation occurring more easily as the temperature is increased, Figure 2. Experimental crack growth data have been fit by the method of least squares to the following empirical equation:

$$v = v_0 \exp [(-E^* + bK_I)/RT] \quad (11)$$

where v_0 , E^* and b are empirical constants of the fit. A summary of these constants is given in Table 1.

Data collected on other commercial glasses as a function of temperature in vacuum could also be fit to eqn. 11 [30]. Subcritical crack growth was observed for glasses that had normal elastic properties, Figure 3. Generally, the slopes, b/RT , obtained for these glasses were higher than those obtained in water (Table 1). High silica content glasses such as silica, chemical borosilicate, and low thermal expansion titania-silica glasses have anomalous elastic properties. These glasses did not exhibit subcritical crack growth in vacuum, even though crack growth was observed when the glasses were tested in water [30,34].

The importance of water to crack propagation in glass was emphasized by recent studies of crack growth in alcohols [31,32]. As is illustrated in Figure 4 for butyl alcohol, the curves obtained in alcohols are similar to those obtained in nitrogen gas containing water. In region I the shift in the crack velocity curves is proportional to the partial pressure of water in the alcohol. Within experimental error, the curve obtained

in fully saturated butyl alcohol is identical to that obtained in water. Similar findings have been obtained for silica glass [33] and for a 7.5% TiO_2 silica glass tested in water saturated air [34]. However, the crack velocities measured on soda-lime-silica glass appears to be slightly higher in water than in water saturated gas (Figure 1).

5. Comparison of Theory and Experiment

Consistency between theory and experiment require predictions from reaction rate theory to agree with experimental measurements of the dependence of crack growth rate on temperature, stress intensity factor and concentration of reactive species in the environment. As will be shown, reasonable predictions of behavior are obtained in all three cases.

5.1 Dependence of Crack Propagation Rate on Concentration

Under the influence of chemical environment the rate of crack propagation is predicted to be proportional to the concentration of reactive species times the reaction rate constant. For water attack on glass in a liquid or gaseous environment, the crack velocity is given by the following equation:

$$v = v_0 [H_2O] k_r \quad (12)$$

where $[H_2O]$ is the concentration of water in the environment, and v_0 is a proportionality constant that incorporates the frequency factor and the concentration of active sites at the crack tip. Since $[H_2O] = a_w/f_w$, where a_w is the chemical activity of the water in the environment, and f_w is the activity coefficient, the crack velocity is predicted to be proportional to the chemical activity of the reacting species. In gases, the chemical activity is proportional to the partial pressure of water vapor so that the crack growth rate should be proportional to the partial pressure of water in the gas. This prediction is confirmed by crack growth studies in soda-lime-silica glass [29], in which the crack velocity is found to be proportional to the partial pressure, p , of water vapor in the gas for a wide range of partial pressures. At low partial pressures of water, however, the crack growth rate is proportional to $p^{1/2}$, suggesting

a possible change in fracture mechanism. Freiman [31] has recently obtained similar results for crack growth in alcohols containing varying amounts of water in solution.

The finding that water saturated liquid or gaseous environments give the same crack propagation curve for region I crack growth data is also consistent with reaction rate theory. To demonstrate this point, we note that $[H_2O] = 1$ for water. In addition, $k_r \propto \exp(\mu_{ow}/RT)$, where μ_{ow} is the chemical potential of water in its standard state. From eqn. 12:

$$v \propto v_0 \exp(\mu_{ow}/RT) \quad (13)$$

For the water saturated environment $[H_2O]_s = a_s/f_s$, where a_s and f_s are, respectively, the activity and the activity coefficient of water in the saturated environment. Since f_s of the water concentration term in eqn. 12 cancels with f_s in eqn. 1, the crack velocity is given by:

$$v \propto v_0 a_s \exp(\mu_{os}/RT), \quad (14)$$

where μ_{os} is the chemical potential of water in the saturated solution referred to its standard state.

At saturation, the chemical potential of the water and the water saturation solution are identical:

$$\mu_{ow} = \mu_s = \mu_{os} + RT \ln a_s \quad (15)$$

By substituting eqn. 15 into eqn. 14, we obtain eqn. 13, which shows that the crack velocity in water saturated environments should be identical to that in water for a given applied stress intensity factor.

Lest the impression be left that the curves for saturated environments are the same over the entire range of crack growth behavior, we note that region II in different environments occurs at different crack velocities. Region II appears to be more dependent on the absolute concentration of the water in the environment rather than on its chemical potential [32]. Thus, the plateau for water saturated nitrogen occurs at $\sim 3 \times 10^{-4}$ m/s; the plateau for water saturated butanol occurs at $\sim 10^{-4}$ m/s; and the plateau for water saturated decanol occurs at $\sim 10^{-6}$ m/s. The plateau for pure water occurs at $\sim 10^{-1}$ m/s, but is the result of viscous drag on the crack surfaces rather than a limit on the rate of transport of water to the crack tip [35].

5.2 Dependence of Crack Propagation Rate on Stress Intensity Factor

For chemical reaction rate theory to be consistent with empirical observations of crack propagation in glass, the term containing the stress intensity factor in eqn. 10 must be set equal to the term containing the stress intensity factor in eqn. 11. This equality leads directly to an expression for the volume of activation in terms of the crack-tip radius and the slope of the crack propagation curve:

$$\Delta V^\ddagger = (b/2) (\pi r)^{1/2} \quad (16)$$

As shown in Table 1 values of b for glass determined from crack propagation studies in water range from ~ 0.110 to ~ 0.216 m^{5/2}/mol, which corresponds to activation volumes ranging from ~ 2.3 cm³/mol for soda-lime-silica glass to ~ 4.3 cm³/mol for silica glass. This calculation assumes $r = 0.5$ nm which corresponds roughly to the size holes expected in the glass network structure.

The degree of bond stretching can be estimated from the activation volume by assuming that stretching occurs along an axis of a cylinder of constant

cross section. The cross section of the Si-O bond in glass can be taken to be the mean of the cross sections of the Si and O atoms which are calculated from the radius r of these atoms in glass ($r_{Si} = 0.04$ nm; $r_O = 0.14$ nm [36]). The equation used by Hamann [22] to calculate the bond elongation occurring as the bond passes through the activated state is:

$$\Delta V^\ddagger = N_A \pi (r_{Si}^2 + r_O^2) \delta l / 2 \quad (17)$$

where N_A is Avogadro's number. Using this formula, values for δl of ~ 0.1 nm and ~ 0.2 nm are calculated for soda-lime-silica glass and for silica glass, respectively. Thus, the degree of strain based on the unstressed bond length of 0.16 nm ranges from ~ 63 to 131 percent. This degree of stretching is similar to that estimated for organic molecules undergoing free radical or molecular dissociations [22].

Based on crack propagation data collected in vacuum, the activation volume for crack growth and the degree of stretching in vacuum are much larger than that just calculated for crack growth in a moist environment. For soda-lime-silica glass, for which the only network former is SiO_2 , $b = 0.88$ $m^{5/2}/mol$, and the activation volume determined from eqn. 16 is ~ 16 cm^3/mol , which is 8 times that found for crack propagation in water. Although this value is at the high range of that reported in the literature for activation volumes, it is not excessively high. The degree of bond stretching that is calculated from eqn. 17 is 0.8 nm, which is approximately 5 times the normal Si-O bond length in the unstretched state. This high degree of stretching is probably unrealistic and results from the assumption that only the crack-tip Si-O bond participates in the bond rupture. If interatomic interactions are such that the bond rupture is a cooperative process (i.e., a wide cohesive region around the crack tip), then the activation volume corresponds to interactions throughout the cohesive region as well as to the displacement of the crack-tip bond.

One possible explanation for the large activation volume for the vacuum data results from the fact that the Si-O bond has a partial ionic character, 37 percent [37], so that long range coulombic forces have to be overcome for fracture to occur. Water molecules, by reacting with the Si-O bonds at the crack tip, partially cancel coulombic attraction since the OH bond is also partially ionic, 29 percent. Thus, in water only short range valence bonds would have to be overcome for bond rupture to occur, and the degree of bond stretching in water would be less than that in vacuum.

Another explanation for the large activation volume may be electrostriction effects, which are known to accompany chemical reactions in liquids. These effects arise as a result of an electrostatic interaction between charged chemical species and the dielectric medium in which the reaction takes place. Using the Born [38] approximation for the change in Gibbs free energy required to transfer a charge of magnitude Ze from a vacuum to a medium having a dielectric constant D , the molar volume change, ΔV_{es} , resulting from electrostatic interactions between the charged species and the medium is given by [20]:

$$\Delta V_{es} = (N_A Z^2 e^2 / 2r) \left[\frac{\partial D^{-1}}{\partial P} + (1 - D^{-1}) \frac{\partial \ln r}{\partial P} \right] \quad (18)$$

where P is the applied pressure and r is the radius of the charge. For reactions in liquids $\partial \ln r / \partial P$ is always negative, and $\partial D^{-1} / \partial P$ is usually negative [20]. Consequently, ΔV_{es} has a negative value in liquids if charges are created, but a positive value if charges are destroyed during the reaction. The electrostatic contribution to the activation volume is found to range from ~ -10 to $-30 \text{ cm}^3/\text{mol}$ in most solvents.

Although electrostrictive forces are also expected to occur in solids, the effect will be quite different from that occurring in solution. First, the bulk modulus of solids is approximately 100 to 1000 times greater than that of liquids, so that the second term of eqn. 18, which depends on the compressibility of the medium, will be very much smaller in solids than it is in solutions and can probably be ignored in the calculation of ΔV_{es} . Second, the dielectric constant of solids decreases with increasing pressure [39], which means that the first term in eqn. 18 will be positive, instead of negative as it is for liquids. Consequently, charge formation in solids results in a positive activation volume. The magnitude of the effect can be estimated from eqn. 18 for the scission of Si-O bonds. From work by Reitzel [40] on silica glass, $\partial D^{-1}/\partial P$ is approximately $4 \times 10^{15} \text{ m}^2/\text{N}$. Assuming that unit electric charges (i.e., $Z = 1$) are formed on both the silicon and oxygen atoms as the bond between these atoms breaks, ΔV_{es} is equal to $\sim 2 \text{ cm}^3/\text{mol}$ for oxygen and $7 \text{ cm}^3/\text{mol}$ for silicon. The combined volume change $\sim 9 \text{ cm}^3/\text{mol}$ is approximately 56 percent of the total activation volume for fracture.

The effect of electrostriction is to partition the volume of activation between the crack-tip bond and the rest of the solid surrounding the crack tip. For Si-O, the activation volume associated with the crack-tip bond is approximately $7 \text{ cm}^3/\text{mol}$ which corresponds to a δ^0 of $\sim 0.35 \text{ nm}$. This value is 2.2 times the normal Si-O spacing and is more reasonable than the value quoted earlier. Consequently, electrostriction seems to play an important role in the fracture of brittle materials, as it does in chemical reactions carried out in solutions.

5.3 Zero Stress Activation Energy Term

When stresses are completely removed from a specimen containing a crack, chemical reactions can still occur at the crack tip. The activation energy for crack motion is then given by the zero stress intensity factor portion of the activation free energy for crack growth, eqn. 10. If the concentration of reactant at the crack tip also depends on temperature, its temperature dependence will have to be added to the activation free energy for crack growth. The sum of these two terms should be equal to E^* (eqn. 11), which is an empirical measurement of the zero stress activation energy for crack growth:

$$\Delta E^\ddagger - [(\gamma^\ddagger V^\ddagger - \gamma V)/\rho] + n \Delta H_1 = E^* . \quad (19)$$

The term $n\Delta H_1$ is the temperature dependence of the concentration of reactive species, and is determined by chemical reactions within the solution, or between the solution and the crack surface, or on the crack surface near the crack tip. The temperature dependence of the concentration of reactive species will therefore be determined by the equilibrium constants of these reactions, which have an Arrhenius dependence on temperature. Measurements of the OH^- ion concentration of slurries of ground glass in water [41], for example, indicate a temperature dependence given by the following relation:

$$[\text{OH}^-] = A \exp (\Delta H_1/RT) \quad (20)$$

If the crack tip reaction is n^{th} order with regard to the active species in solution, then the term to be added to the zero stress activation energy is $n\Delta H_1$, as indicated in eqn. 19.

Equation 19 can be used to compare crack propagation data with corrosion rates that occur at normally unstressed surfaces. Based on the theory presented earlier, ΔE^\ddagger is the activation energy for corrosion at a free surface. Consequently, by evaluating E^* , ΔH_1 and the surface curvature terms of

eqn. 19, ΔE^\ddagger can be evaluated from crack growth data. The value of ΔE^\ddagger so obtained can then be compared with independent measurements of corrosion rates in the reactive environment of interest. Since all of the necessary data is available, comparison of this sort will be made for the attack of hydroxyl ions on the network structure of glass in alkaline environments.

Experiments have shown that at a pH greater than 9, hydroxyl ions directly attack the network structure of glass to cause corrosion [42,43]. Hubbard and Hamilton [42] measured the activation energy for the corrosion of a variety of glass in a 5 percent solution of NaOH in water, and obtained values of the activation energy that ranged from 15.3 to 19.7 kcal/mol. The order of the reaction was not studied specifically. For purposes of this paper, a first order reaction, $n = 1$, will be assumed.

In order to determine the probable pH at crack tips in glass, measurements were made on slurries of water and glass [41]. The pH determined on four of the glasses shown in Table 1 were high enough for direct attack of hydroxyl ions on the network structure of the glass. Values of ΔH_1 , obtained from temperature studies on these glasses are shown in Table 2.

The surface tension term can be evaluated directly from crack propagation data. At the stress corrosion limit, the corrosion rate of the glass at the crack tip will be identical to that occurring at a free surface, so that the crack will not increase in length relative to the surface, and catastrophic fracture will not occur. The condition for the stress corrosion limit is obtained by equating the surface curvature term and

the stress intensity factor term in eqn. 10:

$$[2K_{ISCC}/(\pi a)^{1/2}] \Delta V^\ddagger = -[(\gamma^\ddagger V^\ddagger - \gamma V)/\rho] \quad (21)$$

or using the equality between the stress intensity factor terms in eqns. 10 and 11:

$$bK_{ISCC} = -[\gamma^\ddagger V^\ddagger - \gamma V]/\rho \quad (22)$$

Soda-lime-silica glass is observed to undergo a rapid decrease in crack velocity at stress intensity factors that are slightly greater than $0.25 \text{ MPa}\cdot\text{m}^{1/2}$ and it is believed that this decrease in velocity indicates an approach to a fatigue limit for this glass. Assuming $K_{ISCC} \approx 0.25 \text{ MPa}\cdot\text{m}^{1/2}$, $bK_{ISCC} \approx 2.75 \times 10^4 \text{ J/mol}$ (6.6 kcal/mol). This value can be used to estimate the change of surface energy during the fracture process. Since $\Delta V^\ddagger \approx 2 \text{ cm}^3/\text{mol}$, and since $V \approx 25 \text{ cm}^3/\text{mol}$ for soda-lime-silica glass, an estimate for the right hand side of eqn. 22 can be obtained by using a mean value for the molar volume terms. Assuming $V^\ddagger = V = 25 \text{ cm}^3/\text{mol}$, and $\rho = 0.5 \text{ nm}$, it follows that $\gamma - \gamma^\ddagger \approx 0.55 \text{ J/m}^2$.

Estimates of the corrosion rate of glass in basic solutions are presented in Table 2, using measured values of ΔH_1 , and E^* . In the absence of additional data on the stress corrosion limit in the glasses studied, it is assumed that the surface tension term of eqn. 19 is the same for the four glasses shown in Table 2. The activation energies for corrosion calculated from crack propagation data fall within the range measured by Hubbard and Hamilton [43]. This favorable comparison supports the arguments presented in this paper that crack growth in brittle materials can be explained in terms of chemical reaction rate theory.

6. An Atomic Model of Crack Growth

In previous sections of this paper, the material surrounding the crack tip was treated as if it were a continuum, a procedure that may be questioned when dimensions of the order of the atomic spacing are being considered. In this section, a somewhat simplified atomistic model of fracture is applied to the problem of chemical reactions at crack tips. It is shown that the assumptions used in previous sections of the paper are valid for estimating the activation volume for crack growth. In addition, the partitioning of energy between the internal energy of the crack-tip bond, and work terms that involve the remainder of the solid is shown to be applicable.

The atomistic model of the crack used in this section of the paper (Figure 5) was proposed first by Fuller and Thomson [13,14]. This quasi-one-dimensional model of a crack consists of two semi-infinite chains of atoms that maintain their rigidity by means of an interatomic interaction which is modelled as a flexural force with a force constant β . The chains of atoms are bonded together by a series of cohesive interactions that are modelled as stretchable spring elements between the atom pairs. A crack is formed by assuming that the first n stretchable elements are ruptured, or stretched beyond their range of interaction. With the exception of the crack-tip element, the remaining cohesive-spring elements are assumed to be in the linear regime of their force-displacement response with a spring constant α . The crack-tip element is assumed to be a non-linear element, which reflects the inherent cohesive strength of the solid. A transverse opening force, F , is applied to the end atoms of each chain to force the crack open.

The total potential energy of this crack system is given by [14]:

$$U = -F\delta_0 + \frac{1}{4} \beta \sum_{j=1}^{\infty} [\delta_{j-1} - 2\delta_j + \delta_{j+1}]^2 + n U_{BB} + U_b(\delta_n) + \frac{1}{2} \alpha \sum_{j=n+1}^{\infty} \delta_j^2 \quad (23)$$

where the first term on the right-hand side is the potential energy of the loading system; the second term is the strain energy stored in the flexural bonds; and the remaining terms are the contributions from the cohesive bonds across the crack. These cohesive contributions are, respectively, the total bond energy from the n ruptured bonds, the bond energy of the nonlinearly strained bond at the crack tip, and the linear-elastic strain energy of the remaining cohesive bonds. From a fracture mechanics viewpoint, this potential energy provides both the driving force for fracture and the resistance force to fracture. The crack driving force is derived from the stored elastic strain energy which is released upon crack advance; whereas, the resistance to fracture is contained in the cohesive-bond energy of the crack-tip bond that must be ruptured to advance the crack.

In contrast to the Griffith continuum analysis, where the fracture resistance is provided by the average cohesive energy required to form a new element of surface, the atomistic treatment reveals a fine structure in this process through the discrete nature of the bond rupture event. To illustrate this atomistic influence, the variation of the system potential energy is examined as the crack-tip bond ruptures. For each crack-tip bond displacement, δ_n , the remaining atoms of the solid are required to be in an equilibrium configuration with respect to this displacement. Necessary conditions for these equilibrium configurations are:

$$(\partial U / \partial \delta_j) = 0, \quad \text{for } j \neq n \quad (24)$$

which correspond to an infinite set of fourth-order difference equations. Analytical solutions of these equations are obtainable [14] in the functional form $\delta_j(F, n, \delta_n)$. Substitution of these equilibrium-displacement solutions into eqn. 23 reduces the system potential energy to an explicit function of both the applied fracture mechanics parameters (load and crack length) and the crack-tip bond displacement δ_n :

$$U(F, n, \delta_n) = n U_{BB} - (F^2/6\beta) (2n^3 + 3n^2\xi + n) - K\delta_n/\xi + U_b(\delta_n) + \frac{1}{2} \alpha \left(\frac{\xi-1}{2}\right) \delta_n^2 \quad (25)$$

where ξ is an elastic coefficient defined by $\xi^2(\xi^2-1) = (2\beta/\alpha)$, and $K = (n+\xi)F$ is an effective one-dimensional "stress intensity factor".

This expression is particularly useful for demonstrating the origin of the atomistic energy barrier to intrinsic bond rupture and crack advance. Focusing attention on the n^{th} bond, the first two terms on the right-hand side of eqn. 25 are constant for a given applied force and will not be considered further. The next term, $-K\delta_n/\xi$, corresponds to the reduction in potential energy that results from the applied fracture driving force as the crack-tip bond ruptures. The two remaining terms represent the resistance of the system to the rupture of the crack-tip bond. The first of these resistance terms, $U_b(\delta_n)$, corresponds simply to the interatomic interaction between the crack-tip atoms; whereas the second term, $\frac{1}{2} \alpha \left(\frac{\xi-1}{2}\right) \delta_n^2$ is more subtle and corresponds to the harmonic restoring potential exerted on the crack-tip atoms by the remainder of the (linear elastic) structure. It is the balance between these last three terms that determines the atomistic energy barrier, as is illustrated graphically in Figure 6. The individual

terms are plotted in Figure 6a and their sum is shown in Figure 6b. Clearly, the stress intensity factor term, $-K\delta_n/\xi$, biases the bond rupture to make the final state the more stable configuration in this example.

An important part of the above construct is that the interatomic potential between the crack-tip atoms is decoupled from the interactions of the rest of the solid. This construct provides a model whereby an arbitrary bond-rupture reaction can be studied in an equivalent linear-elastic continuum of crack-tip stiffness $\propto(\frac{\xi-1}{2})$. In particular, the construct can be used to study the effect of chemical reactions on crack propagation, in which case, a modified cohesive force law is substituted for the interatomic potential of the crack-tip atoms. The initial and final equilibrium configuration in Figure 6b now correspond to unreacted and reacted states of the bond respectively. The unstable configuration corresponds to the activated complex of the reaction. The exact influence of the chemical reaction on the rupture of the crack-tip bond depends on the details of the chemical reaction and its activation barrier. Various possibilities have been considered in a recent manuscript [18]. The main effect of the chemical reaction is to further bias the intrinsic activation energy barrier and to allow crack growth to occur at a lower applied stress. An important conclusion of this work is that the thermodynamic surface energy, which determines the thermodynamic condition for crack propagation, is lowered to that of the chemically reacted surface.

The construct can also be used to estimate the activation volume for fracture. Consider the two equilibrium configurations corresponding to the initial

stable configuration (unruptured, crack-tip bond) and to the saddle-point configuration in the potential energy curve (the activated state for the crack-tip bond). The bond displacement at these two configurations are denoted by δ_{no} and δ_n^\ddagger , respectively (Figure 6b). The energy barrier, ΔU_+ , required to reach the activated complex is given by:

$$\begin{aligned} \Delta U_+ &= U(F, n, \delta_n^\ddagger) - U(F, n, \delta_{no}) \\ &= [U_b(\delta_n) - \delta_n \frac{dU_b}{d\delta_n} - \frac{1}{2} \alpha \left(\frac{\xi-1}{2}\right) \delta_n^2] \Big|_{\delta_{no}}^{\delta_n^\ddagger} \end{aligned} \quad (26)$$

where the energies in each equilibrium configuration, $U(F, n, \delta_n^\ddagger)$ and $U(F, n, \delta_{no})$, are obtained from eqn. 25. The dependence of this activation energy barrier on the fracture driving force, K , is obtained by taking the derivative of eqn. 26 with respect to K (utilizing the stability condition of each state to obtain the K dependence of δ_{no} and δ_n^\ddagger):

$$\frac{d(\Delta U_+)}{dK} = - (\delta_n^\ddagger - \delta_{no}) \xi^{-1} \quad (27)$$

Since K has units of force in the simple atomistic model used in the present construct, an applied crack-tip stress can be defined by dividing K/ξ by the effective area, A , of the bond at the crack tip, Figure 7:

$$\sigma = K/(\xi A) \quad (28)$$

Substituting this relation into eqn. 27, the following relation is obtained:

$$\frac{d(\Delta U_+)}{d\sigma} = - A (\delta_n^\ddagger - \delta_{no}) \equiv -\Delta V^\ddagger \quad (29)$$

where ΔV^\ddagger is the activation volume for the crack-tip reaction. This definition of ΔV^\ddagger is identical to that used in the literature of chemical reaction rate theory. Thus, it has been shown that an atomistic model of crack growth is consistent with a model of crack growth derived by

treating the crack tip as an elastic continuum. This finding supports the assumption that crack-tip stresses can be treated by a continuum approach to fracture.

REFERENCE

1. B. J. Hockey and B. R. Lawn, *J. Mater. Sci.* 10, 1275 (1975).
2. B. R. Lawn, B. J. Hockey and S. M. Wiederhorn, *J. Mat. Sci.*, in press (1980).
3. J. Dunning and D. Dunn. *Geol. Soc. of Amer.*, Annual Meeting, Toronto, Abstract with Programs, 10 [7], 395 (1978).
4. S. M. Wiederhorn and P. R. Townsend, *J. Am. Ceram. Soc.* 53, 486 (1970).
5. S. M. Wiederhorn, *J. Am. Ceram. Soc.* 52, 99 (1969).
6. R. J. Jaccodine, *J. Electrochem. Soc.* 110, 524 (1963).
7. W. B. Hillig, "The Factors Affecting the Ultimate Strength of Bulk Fused Silica," Symposium sur la Resistance Mecanique du Verre et les Moyens de l'Amelioration, Union Scientifique Continentale du Verre, Charleroi, Belgium, (1962).
8. B. A. Proctor, I. Whitney and J. W. Johnson, *Proc. Roy. Soc. A* 297, 534 (1967).
9. D. A. Stuart and O. L. Anderson, *J. Am. Ceram. Soc.* 36, 416 (1953).
10. S. M. Cox, *J. Glass. Tech.* 32, 127T (1948).
11. B. R. Lawn, *J. Mater. Sci.* 10, 469 (1975).
12. G. M. Bartenev and I. V. Razumovskaya, pp 1871-80, in *Proc. 1st Int. Conf. on Fracture*, Vol. 3, Sendai, Japanese Society for Strength and Fracture of Materials (1966).
13. E. R. Fuller, Jr. and R. M. Thomson, "Nonlinear Lattice Theory of Fracture," pp 387-394 in *Fracture 1977*, Vol. 3, edited by D. M. R. Taplin, Univ. of Waterloo Press, Canada, (1977).
14. E. R. Fuller, Jr. and R. M. Thomson, "Lattice Theories of Fracture," pp 507-548 in *Fracture Mechanics of Ceramics*, Vol. 4, edited by R. C. Bradt, D. P. H. Hasselman, and F. F. Lange, Plenum Publishing Corporation, (1978).
15. E. R. Fuller, Jr. and R. M. Thomson, "Theory of Chemically Assisted Fracture," pp 485-494, in *Proceedings of the Third International Conference on Mechanical Behaviour of Materials*, Vol. 2, edited by K. J. Miller and R. F. Smith, Pergamon Press, (1979).
16. R. Thomson, *J. Mat. Sci.*, in press (1980).
17. E. R. Fuller, Jr. and R. M. Thomson, *J. Mat. Sci.* in press (1980).

18. E. R. Fuller, Jr., B. R. Lawn, and R. M. Thomson, "Atomic Modelling of Crack-Tip Chemistry," submitted to Acta Met.
19. K. J. Laidler, Chemical Kinetics, McGraw-Hill Book Co., New York (1965).
20. G. Kohnstam, Kinetic Effects of Pressure, pp 355-408 in Progress in Reaction Kinetics, G. Porter, Editor, Pergamon Press, London (1970).
21. M. G. Evans and M. Polanyi, Trans. Faraday Soc. 42, 875 (1935).
22. S. D. Hamann, "Chemical Kinetics," pp 163-207 in High Pressure Physics and Chemistry, R. S. Bradley ed., Academic Press, London (1963).
23. C. A. Eckert, Ann. Rev. Phys. Chem. 23, 239 (1972).
24. R. J. Charles and W. B. Hillig, pp 511-527 in ref. 7.
25. S. M. Wiederhorn and L. H. Bolz, J. Am. Ceram. Soc. 53, 543 (1970).
26. A. W. Adamson, Physical Chemistry of Surfaces, Interscience Publishers New York (1967).
27. S. M. Wiederhorn, Int. J. Fract. Mech. 4, 171 (1968).
28. P. F. Becker and S. W. Freiman, J. Appl. Phys. 49, 3779 (1978).
29. S. M. Wiederhorn, J. Am. Ceram. Soc. 50, 407 (1967).
30. S. M. Wiederhorn, H. Johnson, A. M. Diness and A. H. Heuer, J. Am. Ceram. Soc. 57, 336 (1974).
31. S. W. Freiman, J. Am. Ceram. Soc. 57, 350 (1974).
32. S. W. Freiman, S. M. Wiederhorn and C. J. Simmons, J. Am. Ceram. Soc., submitted for publication.
33. S. M. Wiederhorn, unpublished data.
34. S. M. Wiederhorn, A. G. Evans, E. R. Fuller and H. Johnson, J. Am. Ceram. Soc. 57, 319 (1974).
35. T. A. Michalske and V. D. Frechette, "Dynamic Effects of Liquids on Crack Growth Leading to Catastrophic Failure in Glass", J. Am. Ceram. Soc. to be published.
36. B. A. Proctor, Appl. Mat. Res. 3, 28 (1964).
37. M. F. C. Ladd, Structure and Bonding in Solid State Chemistry, Ellis Harwood Limited Chichester (1979).
38. M. Born, Z. Physik., 1, 45 (1920).

39. R. S. Bradley, "Other Miscellaneous Effects of Pressure," pp 325-37 in High Pressure Physics and Chemistry, Vol. 2, R. S. Bradley, ed. Academic Press, London (1963).
40. J. Reitzel, Nature, Lond. 178, 940 (1956).
41. S. M. Wiederhorn, J. Am. Ceram. Soc. 55, 81 (1972).
42. R. W. Douglas and T. M. M. El-Shamy, J. Am. Ceram. Soc., 50, (1967).
43. D. Hubbard and E. H. Hamilton, J. Res. Nat. Bur. Stand., 27 143 (1941).
44. S. M. Wiederhorn, "Subcritical Crack Growth in Ceramics," pp 613-646 in Fracture Mechanics of Ceramics, Vol. 2, R. C. Bradt, D. P. H. Hasselman and F. F. Lange eds. Plenum Publishing Corp. New York (1974).

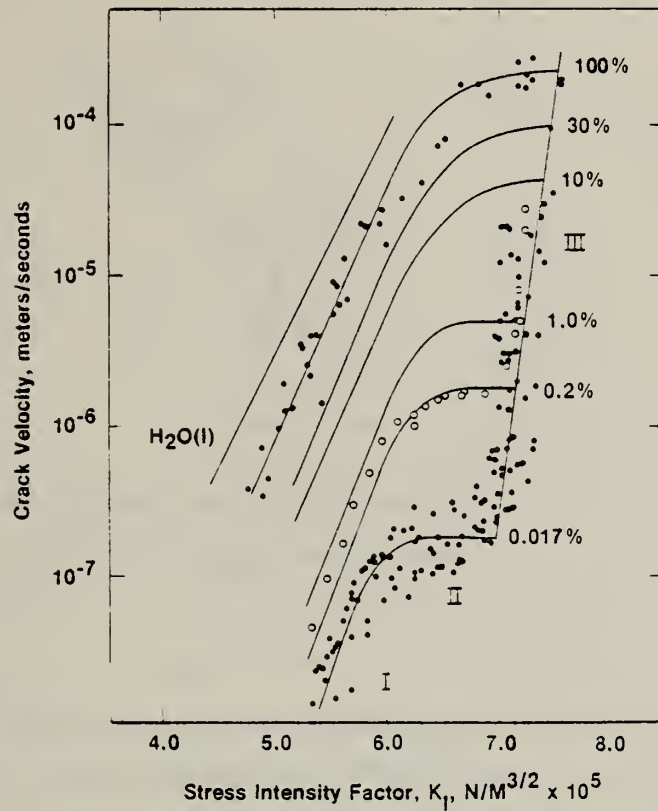
Table 1 - Summary of Stress Corrosion Data

Environment	Glass	E* kcal/mol (kJ/mol)	b (m ^{5/2} /mol)	ln v ₀
Water [25]	Silica	33.1 (139)	0.216	-1.32
	Aluminosilicate I	29.0 (121)	0.138	5.5
	Aluminosilicate II	30.1 (126)	0.164	7.9
	Borosilicate	30.8 (129)	0.200	3.5
	Lead Alkali	25.2 (106)	0.144	6.7
	Soda-Lime-Silica	26.0 (109)	0.110	10.3
Vacuum [30]	61% Lead	83.1 (348)	0.51	5.1
	Aluminosilicate III	176 (705)	0.77	14.1
	Borosilicate Crown	65.5 (275)	0.26	6.6
	Soda-Lime-Silica	144 (605)	0.88	-5.7

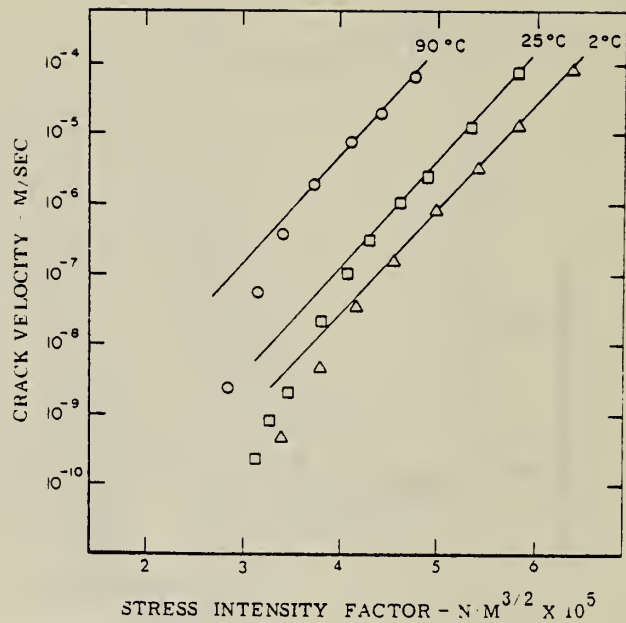
Table 2 - Calculated Activation Energy for Corrosion,
 ΔE^\ddagger , kcal/mol

Glass	E^*	$(\gamma^\ddagger v^\ddagger - \gamma v)/\rho$	ΔH_1	ΔE^\ddagger
Aluminosilicate I	29.0	6.6	4.7	17.7
Aluminosilicate II	30.1	6.6	2.4	21.1
Lead Alkali	25.2	6.6	2.1	16.5
Soda-Lime-Silica	26.0	6.6	1.0	18.4

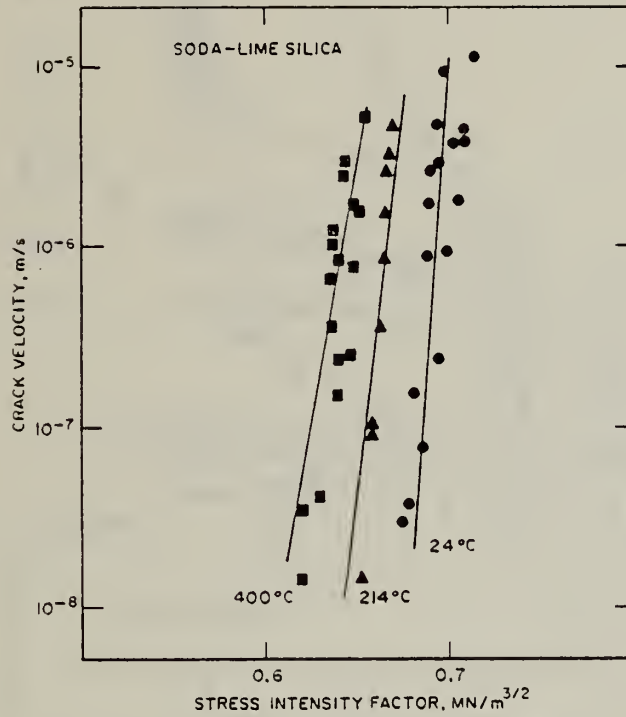
Hubbard and Hamilton [42] $E^\ddagger = 15.3$ to 19.7



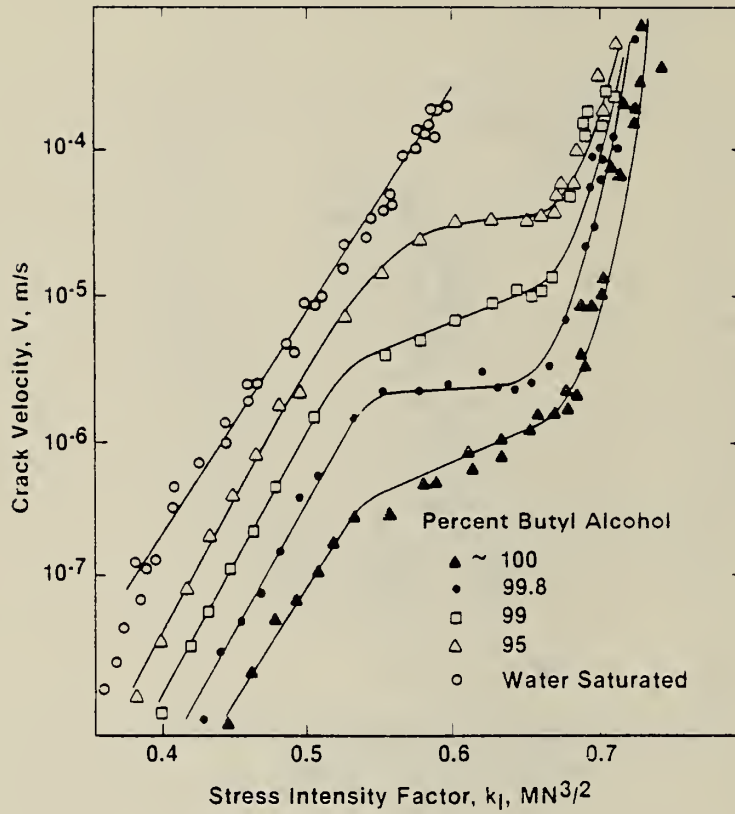
1. Dependence of crack velocity on applied stress intensity factor, soda-lime-silica glass. The percent relative humidity for each set of runs is given on the right-hand side of the diagram. Roman numerals identify the different regions of crack propagation. (Wiederhorn, ref. 43; original data from ref. 29).



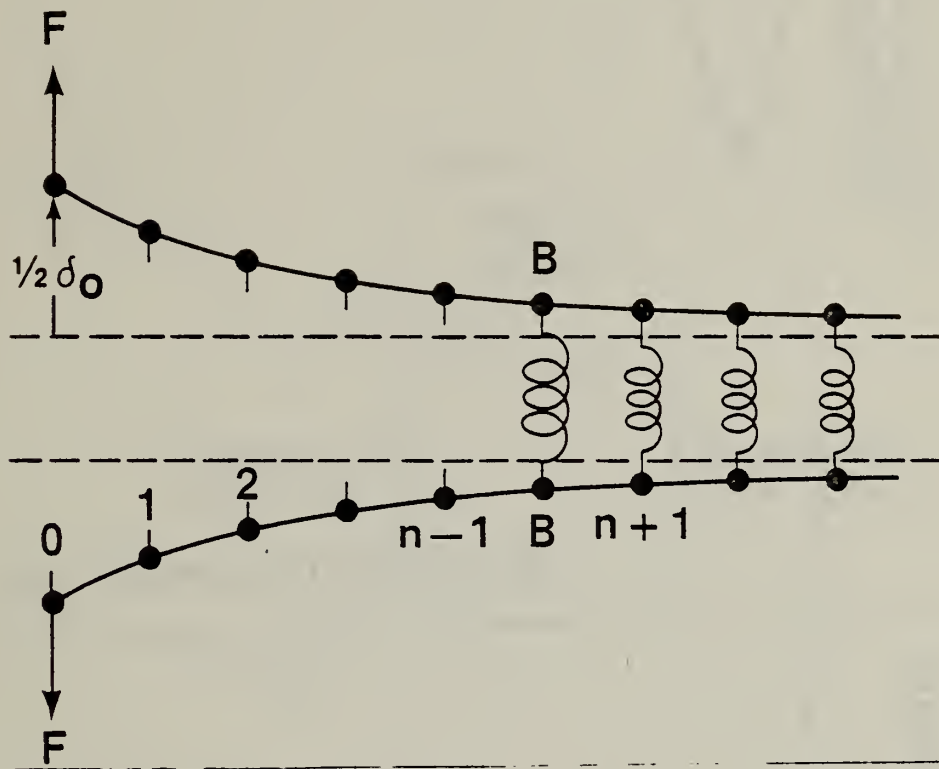
2. Influence of temperature on fracture behavior of glass in water. Some data, such as that given above for soda-lime-silica glass, were curved at low values of K_I , indicating an approach to a static fatigue limit. Other data, such as that for silica, were straight for the entire range of K_I . Curved data were fit by the method of least squares only over the linear portion of the data to obtain the summary given in Table 3. (Wiederhorn, ref. 25).



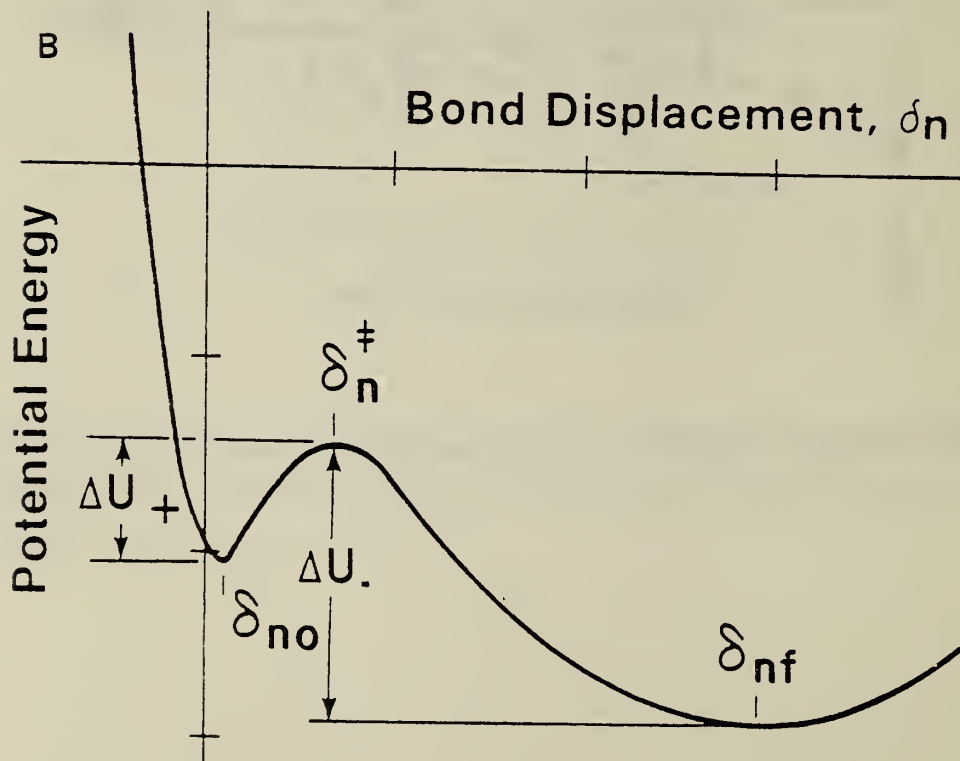
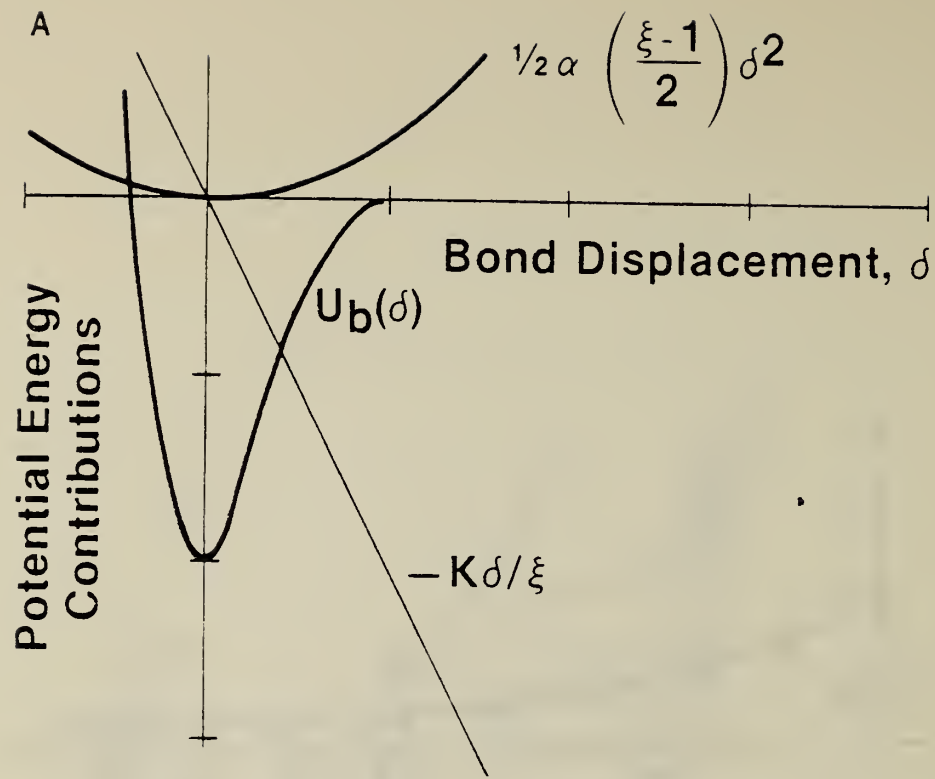
3. Influence of temperature on the fracture behavior of soda-lime-silica glass tested in a vacuum of $\sim 10^{-4}$ torr (10^{-2} Pa). (Wiederhorn, Johnson, Diness and Heuer, ref. 30).



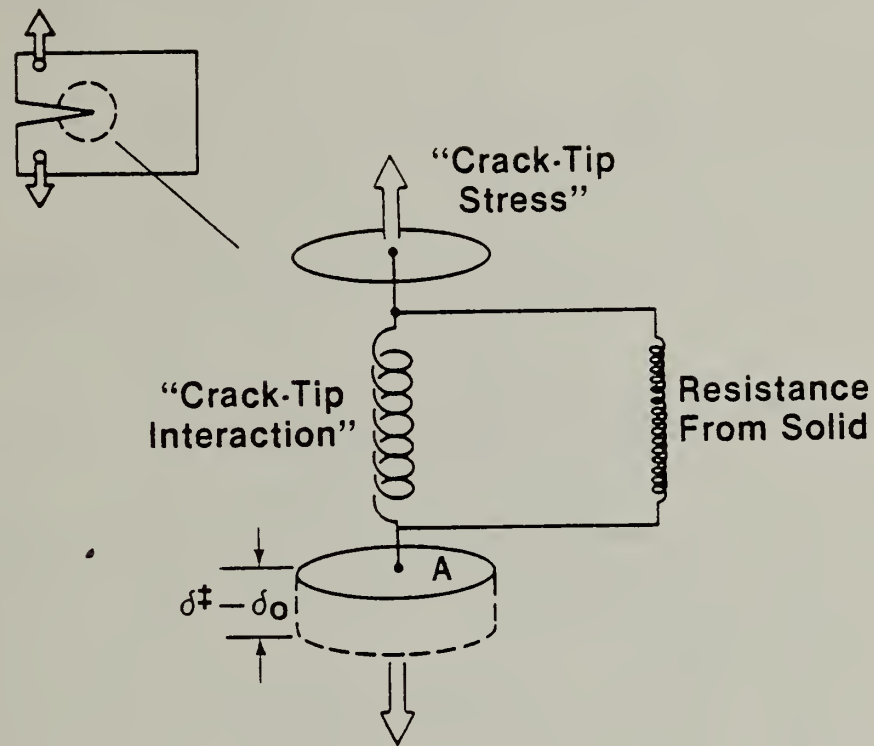
4. Fracture behavior of soda-lime-silica glass tested in butyl alcohol solutions that contained different quantities of dissolved water. (Freiman, Wiederhorn and Simmons, ref. 32.)



5. Atomistic model of crack. (Fuller and Thomson, ref. 13, 14).



6. Schematic diagram of the potential energy terms involved in the atomistic model of fracture shown in figure 5; (a) plot of the three individual potential energy terms; (b) plot of the sum of the three energy terms for a potential barrier for fracture. (Fuller and Thomson, ref. 14).



7. Schematic diagram depicting the applied force for fracture K/ξ , the cross-sectional area, A , of the strained bond and the bond displacement, $\delta_n^\ddagger - \delta_{n0}$, during activation. The figure also depicts the resistance force from the crack-tip bond, $dU_b/d\delta_n$, and the harmonic restoring force, $\alpha(\xi-1)\delta_n/2$, exerted on the crack-tip bond by the remainder of the linear-elastic structure.

U.S. DEPT. OF COMM. BIBLIOGRAPHIC DATA SHEET	1. PUBLICATION OR REPORT NO. NBSIR 80-2023	2. Gov't. Accession No.	3. Recipient's Accession No.
4. TITLE AND SUBTITLE "Micromechanisms of Crack Growth in Ceramics and Glasses in Corrosive Environments"		5. Publication Date MAY 1980	
7. AUTHOR(S) S.M. Wiederhorn, E.R. Fuller, Jr., and R. Thomson		6. Performing Organization Code	
9. PERFORMING ORGANIZATION NAME AND ADDRESS NATIONAL BUREAU OF STANDARDS DEPARTMENT OF COMMERCE WASHINGTON, DC 20234		8. Performing Organ. Report No.	
12. SPONSORING ORGANIZATION NAME AND COMPLETE ADDRESS (Street, City, State, ZIP) Same		10. Project/Task/Work Unit No.	
15. SUPPLEMENTARY NOTES <input type="checkbox"/> Document describes a computer program; SF-185, FIPS Software Summary, is attached.		11. Contract/Grant No.	
16. ABSTRACT (A 200-word or less factual summary of most significant information. If document includes a significant bibliography or literature survey, mention it here.) At normal temperatures and pressures, water is known to have a strong influence on the strength of ceramics and glasses. Behaving as a stress-corrosion agent, water causes these materials to fail prematurely as a consequence of subcritical crack growth. A basic premise of this paper is that stress-corrosion cracking of ceramics is a chemical process that involves a stress-enhanced chemical reaction between the water and the highly stressed ceramic near the crack tip. Plastic deformation is believed to play no role in this fracture process. After a brief survey of chemical reaction rate theory, the basic rate equation from this theory is modified to reflect physical and chemical processes that occur at crack tips. Modification of the rate equation is based on the assumption that the crack tip can be modelled as an elastic continuum, an assumption that is supported by a simple atomistic model of crack growth. When tested against experimental data collected on glass, the theory was found to be consistent with measurements of the crack-growth dependence on temperature, applied stress intensity factor, and concentration of reactive species in the environment.		13. Type of Report & Period Covered	
17. KEY WORDS (six to twelve entries; alphabetical order; capitalize only the first letter of the first key word unless a proper name; separated by semicolons) Ceramics; Glass; Fracture; Strength; Stress-corrosion cracking; Sub-critical crack growth.		14. Sponsoring Agency Code	
18. AVAILABILITY <input type="checkbox"/> Unlimited <input checked="" type="checkbox"/> For Official Distribution. Do Not Release to NTIS <input type="checkbox"/> Order From Sup. of Doc., U.S. Government Printing Office, Washington, DC 20402, SD Stock No. SN003-003- <input type="checkbox"/> Order From National Technical Information Service (NTIS), Springfield, VA. 22161		19. SECURITY CLASS (THIS REPORT) UNCLASSIFIED	21. NO. OF PRINTED PAGES
		20. SECURITY CLASS (THIS PAGE) UNCLASSIFIED	22. Price



